Review

Molecular Probes for Evaluation of Oxidative Stress by In Vivo EPR Spectroscopy and Imaging: State-of-the-Art and Limitations

Nikola Babić [1] and Fabienne Peyrot [1,2,*]

[1] Laboratoire de Chimie et Biochimie Pharmacologiques et Toxicologiques, UMR 8601 CNRS, Université Paris Descartes, Sorbonne Paris Cité, 45 rue des Saints-Pères, 75006 Paris, France; nikola.babic19791@gmail.com

[2] École Supérieure du Professorat et de l'Éducation (ESPE) de l'Académie de Paris, Sorbonne Université, 10 rue Molitor, 75016 Paris, France

* Correspondence: fabienne.peyrot@parisdescartes.fr

Abstract: Oxidative stress, defined as a misbalance between the production of reactive oxygen species and the antioxidant defenses of the cell, appears as a critical factor either in the onset or in the etiology of many pathological conditions. Several methods of detection exist. However, they usually rely on ex vivo evaluation or reports on the status of living tissues only up to a few millimeters in depth, while a whole-body, real-time, non-invasive monitoring technique is required for early diagnosis or as an aid to therapy (to monitor the action of a drug). Methods based on electron paramagnetic resonance (EPR), in association with molecular probes based on aminoxyl radicals (nitroxides) or hydroxylamines especially, have emerged as very promising to meet these standards. The principles involve monitoring the rate of decrease or increase of the EPR signal in vivo after injection of the nitroxide or the hydroxylamine probe, respectively, in a pathological versus a control situation. There have been many successful applications in various rodent models. However, current limitations lie in both the field of the technical development of the spectrometers and the molecular probes. The scope of this review will mainly focus on the latter.

Keywords: electron paramagnetic resonance; electron spin resonance; nitroxyl radical; hydroxylamine; spin probe; oxidative stress; reactive oxygen and nitrogen species

1. Introduction

One of the greatest forthcoming challenges facing developed countries is affording active and healthy aging conditions in their population. Cancer, brain, and cardiovascular diseases, and musculoskeletal conditions are among the largest contributors to morbidity and mortality worldwide, while their prevalence increases with age. Hence, there is an urge for the introduction of new early diagnosis methods and efficient treatments against these debilitating pathologies. These conditions are associated with a large variety of distinct risk factors. For instance, in a number of neurodegenerative diseases, such as Parkinson's, Alzheimer's diseases, and amyotrophic lateral sclerosis (ALS), a specific dysfunctional protein is responsible for neuronal degeneration and the appearance of clinical symptoms. However, it is more and more evident that there are also shared pathological mechanisms that exacerbate disease development, whatever the condition. Indeed, oxidative stress has a major impact on disease susceptibility and contributes to the general weakness of the aged subject. Oxidative stress is defined as a misbalance between the endogenous production of reactive oxygen and nitrogen species (RONS, Figure 1) and the antioxidant defenses at the cellular level, and leads to oxidative damage to proteins, lipids, and DNA. The redox status is reflected in the thiol/disulfide balance since this constitutes the principal cellular redox buffer. In the context of

oxidative stress, protection afforded by potential therapeutic agents could arise from their antioxidant properties and their ability to eliminate RONS in the cell.
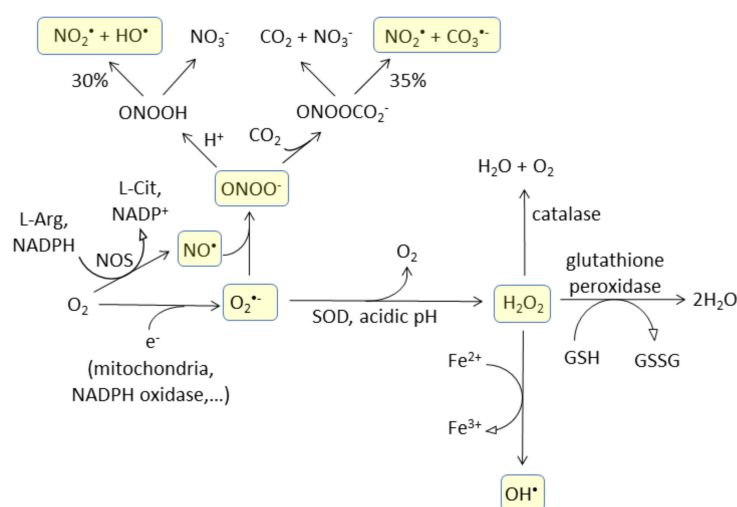
Figure 1. Principal reactive oxygen and nitrogen species (RONS) and a few elimination pathways. (NOS: nitric oxide synthase, L-Arg: L-arginine, L-Cit: L-citrulline, GSH: glutathione, GSSG: glutathione disulfide).

A non-invasive method of the detection and mapping of oxidative stress in vivo would thus afford valuable information on disease development and would help in the design of tools for early diagnosis and treatment. Ideally, the specific identification of the redox chemistry involved in a pathological condition is desired [1]. However, monitoring global modifications in the redox status in vivo is helpful as a complementary technique to more specific ex vivo methods.

EPR spectroscopy has long been a method of choice for the detection of paramagnetic species, such as free radicals or transition metal ions in vitro, but the boost in in vivo EPR spectroscopy and imaging applications in biology and biomedicine is more recent [2,3]. In order to evaluate oxidative stress in vivo by EPR, an injection of exogenous molecular probes essentially based on either aminoxyl radicals (nitroxides) or hydroxylamines is necessary [4]. Then, differences in the rate of the decrease or increase of the EPR signal in vivo after injection of the nitroxide or the hydroxylamine probe, respectively, in a pathological versus a control situation, reflect differences in the redox status (Figure 2). Apart from the probe injection, the invasiveness of the technique is reduced with exposure to low intensity magnetic fields (0.3 T) and low power microwave radiations (<200 mW). EPR also has a competitive advantage over fluorescence or luminescence techniques routinely used to measure RONS in cells and tissues because (depending on the frequency) microwave penetration is enough for whole body in vivo studies of rodents, including the brain, without a need for trepanation. However, to avoid the non-resonant microwave absorption by water contained in living tissues (i.e., the phenomenon which is used to heat food in microwave ovens), the working frequency must be lowered to 1.2 GHz or below (L-band). This leads to a dramatic decrease in sensitivity compared to in vitro experiments at X-band (9.8 GHz).
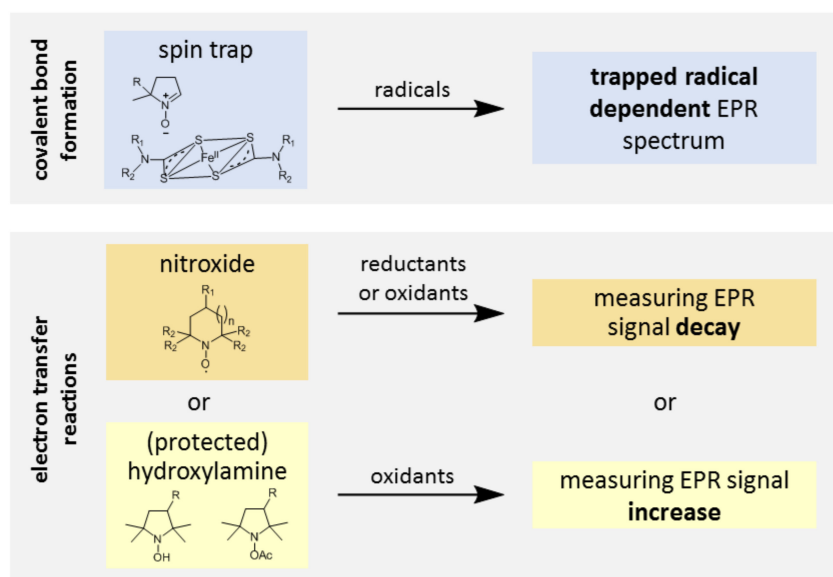
Figure 2. Principle of oxidative stress evaluation by EPR. Molecular probe administration is followed by monitoring of the EPR signal in vivo in a control vs. pathological condition.

EPR spectroscopy in association with molecular probes has been successfully applied to the evaluation of the redox status of tumors [5–10] or in rodent models of diverse pathological conditions, such as hypertension, stroke, epilepsy, and sepsis [11–17]. However, major limitations remain that can be divided into two kinds: technical and chemical. First, time-resolved oxidative stress imaging studies are still impossible with current commercially-available spectrometers due to slow magnetic field sweeping in conventional continuous wave (CW) EPR (15 to 30 min for a bidimensional image, depending on the signal-to-noise ratio, the desired field of view, and the resolution). Indeed, to obtain an EPR image by this method, the accumulation of very large numbers of EPR projections recorded with stepping orientations of the magnetic field gradient to effectively encode spatial information in the EPR spectra is required before signal processing through deconvolution and backprojection. However, recent advances in EPR technology suggest that this technological lock will soon be removed. Pulsed EPR [18], rapid-scan EPR [19], and fast field scanning CW EPR associated with improved image reconstruction procedures [20–22] considerably reduce the acquisition time (tridimensional EPR images with a submillimetric resolution are obtained in one or two minutes). Secondly, available molecular probes are extremely limited in number, they have a poor biostability, and their lack of specificity makes the interpretation of observations difficult. In the present article, we will define the ideal molecular probe for the evaluation of oxidative stress by EPR, describe the limitations of current probes, and review the directions for improvement suggested in the literature.

2. The Ideal Molecular Probe for Evaluation of Oxidative Stress by EPR

The list of characteristics of the ideal probe below follows general rules for molecular probe design; solely the fifth item is specific to EPR probes:

1. The probe is transformed specifically by RONS produced by cells and is not sensitive to reductive processes. The variation of intensity of the EPR signal thus reflects the level of oxidative stress;
2. Metabolization and excretion of the probe are slow compared to the typical time-scale of EPR imaging;
3. The probe is highly water-soluble or can be easily formulated for in vivo administration;
4. The probe distributes to the tissue of interest and accumulates to above the level of detection of the EPR spectrometer. Its compartmentalization corresponds to the site of RONS production;

5. The spectral properties of the probe, especially its EPR linewidth, are compatible with the acquisition of EPR images with a resolution of a few millimeters;
6. The probe is not toxic at the dose required for imaging.

3. Problems to Solve

3.1. Probe Reactivity

Even though key RONS, such as superoxide, hydroxyl radicals, or nitric oxide, are paramagnetic species, their direct detection by EPR is usually prevented by their short lifetime and low steady-state concentration or because of magnetic properties. Detection by EPR in association with spin traps has been developed to circumvent these problems (Figure 3). The radical product of the reaction, the so-called spin adduct, is stabilized compared to the initial radical and accumulates, while the characteristic EPR spectrum of the spin adduct affords unambiguous identification of the trapped radical because a covalent bond is formed during the reaction. Spin trapping is thus the ultimate in selectivity in vitro. However, apart from scarce examples outside physiological relevance [23], in vivo applications of cyclic nitrones are currently prevented by a lack of sensitivity of conventional EPR spectrometers. In the case of a superoxide, for instance, concentrations of spin adducts in vivo are very low because the spin trapping rate by cyclic nitrones is slow ($k < 10^2$ M^{-1} s^{-1}) and outcompeted by endogenous elimination systems (like superoxide dismutase and nitric oxide) and the nitroxide spin adducts are highly unstable in the presence of biological reductants [24–27]. NO imaging using ferrous iron-dithiocarbamate complexes dates back to the early 1990s, but many potential artefacts have been reported since then, related to the spin trap reactivity. We refer the reader to dedicated reviews for further details [28,29].
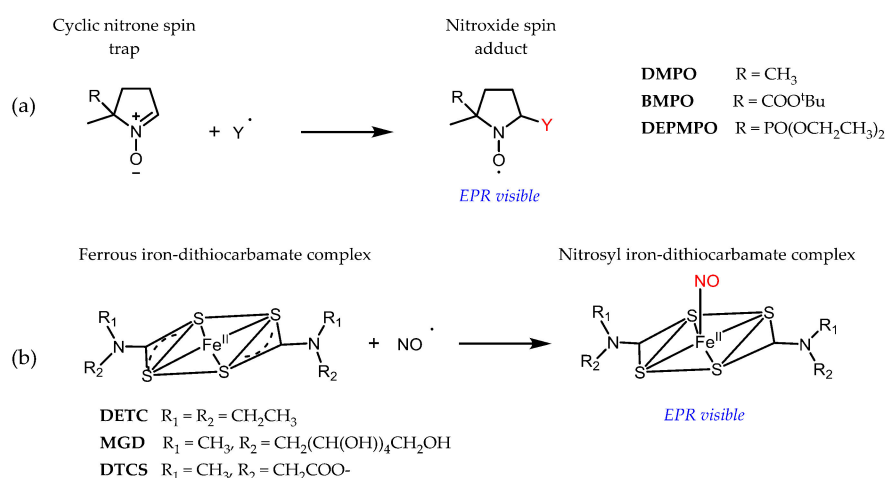
Figure 3. Principle of spin trapping with cyclic nitrone spin traps (a) and ferrous iron-dithiocarbamate complexes (b). In both cases, a covalent bond is formed between the radical and the spin trap.

The main type of molecular probes currently in use in vivo for the monitoring of oxidative stress are nitroxide radicals (Figure 4), especially piperidine or pyrrolidine derivatives. By opposition to nitroxide spin adducts derived from cyclic nitrones, these radicals are almost indefinitely persistent in buffered aqueous solutions, due to the exhaustive substitution of carbons adjacent to the nitrogen by methyl groups and are often referred to as "stable" radicals in the literature. Nevertheless, these radicals can take part in electron-transfer reactions with cellular components and thus report on the redox activity of the cell by shuttling between three oxidation states: the aminoxyl radical (the only EPR detectable species), the hydroxylamine (the reduced form obtained by coupled proton-electron transfer), and the N-oxoammonium cation (the mono-electronic oxidation product) (Figure 4).
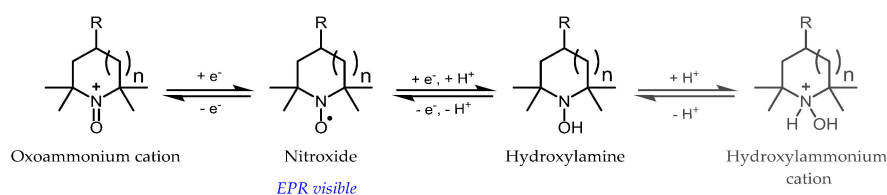
Figure 4. Redox reactions of nitroxides (pyrrolidine, n = 0; piperidine, n = 1); protonation of hydroxylamine to hydroxylammonium cation is also presented.

The biochemistry of tetramethyl-substituted nitroxides has been reviewed elsewhere [30,31]. In brief, after the in vivo injection of nitroxide, a decrease in the EPR signal is observed, mainly due to the reduction to hydroxylamine [32,33]. In normal tissues, this phenomenon is usually attributed to mitochondrial enzymatic reduction, with a potential role of ascorbic acid and, indirectly, thiols [34,35]. Therefore, in tumors, where hypoxic conditions are found with concomitant enhancement of reducing activity, the rate of decay of the nitroxide is increased, reflecting a more reductive environment [5], while in the case of the overproduction of hydrogen peroxide by monoamine-oxidases (MAO) induced by neuroleptics [36], or in ischemia-reperfusion injury [12,20], which depletes the reducing capacity of the brain, the rate of nitroxide decay is decreased compared to the control. However, under some oxidative stress conditions, such as sepsis [14], the rate of decay of the signal also increases, likely due to initial oxidation of the nitroxide to the oxoammonium cation by a superoxide radical [37] or other RONS [38–40], followed by reduction to the hydroxylamine by two-electron reductants, such as NAD(P)H or thiols [37,41]. The acceleration of signal decay then reflects the level of oxidative stress and it is reversed by treatment with antioxidants or inhibitors of RONS-generating enzymes. EPR observations are thus difficult to interpret without a good knowledge of the system under study. To eliminate this ambiguity, it is desirable to prevent the reduction of nitroxide probes by biological reductants (be it small molecules or enzymes) and to make them more selective for oxidation by RONS.

Another approach consists of using cyclic hydroxylamines as molecular probes for oxidative stress [42–45]. In this case, the EPR signal appears along with nitroxide formation in the tissue following oxidation of the probe by RONS (Figure 5). Far from being specific, oxidation occurs primarily upon reaction with a superoxide anion, peroxyl radicals, or peroxynitrite, whereas reaction with hydrogen peroxide is negligible, except in the presence of transition metal ions [46–48]. However, under aerobic conditions, lipophilic hydroxylamines are oxidized by cytochrome c oxidase in membranes, while hydrophilic hydroxylamines are not significantly oxidized by cells [49]. The use of specific inhibitors or scavengers of RONS is required in vitro for clarification of the oxidizing species, but it is more difficult to apply in vivo, so interpretation of the results should be done with caution. Different factors decrease the sensitivity of the technique. Most commonly used hydroxylamine spin probes exist in equilibrium with high proportions of their unreactive protonated forms at a physiological pH (pKa ≈ 7) [45]. Because the product of oxidation of the hydroxylamine spin probe is a nitroxide, it is susceptible to bioreduction, which leads to loss of the EPR signal. Another problem is that for standard tetramethyl-substituted spin probes, the superoxide reacts faster with the nitroxide than with the corresponding hydroxylamine [46], leading to underestimation of the rate of superoxide production at a high level of probe conversion. Because they are susceptible to autoxidation, free hydroxylamines have almost never been used for in vivo EPR and ex vivo analysis is usually preferred [45].
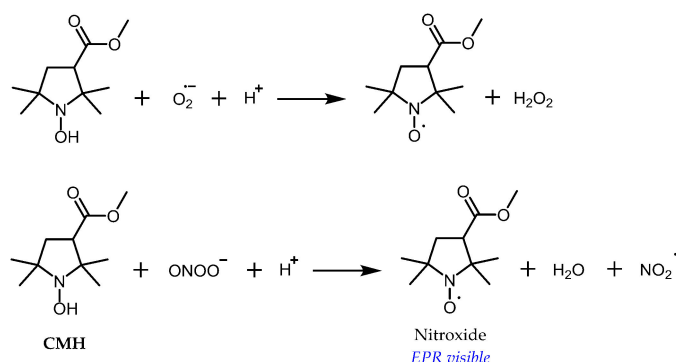
Figure 5. The principle of using hydroxylamines as probes for RONS. Electron-transfer reactions of 1-hydroxy-3-methoxycarbonyl-2,2,5,5-tetramethylpyrrolidine (CMH), the most often used hydroxylamine probe, with superoxide and peroxynitrite.

Alternatives to free hydroxylamines, acyl-protected hydroxylamine spin probes, such as ACP (1-acetoxy-3-carbamoyl-2,2,5,5-tetramethylpyrrolidine), are inert to autoxidation and easier to handle in air prior to use. These compounds require intracellular activation by esterases to release the corresponding reactive hydroxylamine in situ (Figure 6). A very important study using ACP in sepsis model mice induced by lipopolysaccharide (LPS) showed that the signal of the corresponding nitroxide in the chest and upper abdomen increased up to 7–8 min after ACP injection and then decreased; however, this was significantly slower in the LPS-treated compared to healthy mice [16]. Suppressed decay of the in vivo signal in LPS-treated mice was cancelled by either the simultaneous administration of polyethylene glycol-conjugated SOD and catalase or the administration of L-NAME, N(ω)-nitro-L-arginine methyl ester, an NOS inhibitor. Therefore, peroxynitrite rather than a superoxide anion was proposed as the main contributor to hydroxylamine oxidation in LPS-treated mice.
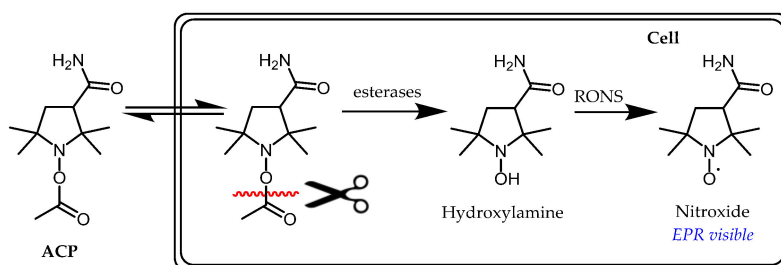
Figure 6. Principle of acyl-protected hydroxylamine spin probes. As with free hydroxylamine, RONS detection is based on an electron-transfer reaction.

The glutathione (GSH) redox status in vivo, characterized by both the GSH concentration and the GSH/glutathione disulfide (GSSG) ratio, is considered as an important biochemical indicator of oxidative stress and a potentially relevant predictive biomarker of tumor response to therapy in the clinic. Typical cytosol GSH concentrations range from 1 to 10 mM and the GSH/GSSG couple represents close to half of the total thiol/disulfide pool in the cell. In normal conditions, reduced GSH highly predominates over the oxidized form (GSH/GSSG ≈ 100 or higher) [50]. A series of lipophilic disulfide-linked dinitroxide spin probes has been proposed to measure GSH and the image thiol redox status in vivo. These probes are paramagnetic versions of Ellman's reagent. Upon reaction with reduced thiols via the thiol-disulfide exchange reaction, the EPR spectrum undergoes a drastic change from the complex spectrum of a biradical with spin exchange to the typical triplet pattern of mononitroxides (Figure 7). Recent versions of these probes include ^{15}N-labelling of the aminoxyl function and perdeuteration to sufficiently increase the signal-to-noise ratio for in vivo application and imaging [51,52]. Interpretation of in vivo EPR results with these probes is far from straightforward for several reasons. The concentration of the probe must be small compared to that of GSH, so as not

to exhaust the reducing equivalents of the cell. Therefore, concentration estimations do not rely on endpoint measurements but on kinetic rate determination, when it has been shown that these rates are highly dependent on local pH and temperature due to the dominant contribution of the thiolate anion GS⁻ in the reaction. Multiparametric measurements are thus required, involving both probes for pH and redox status [10]. Fortunately, protein thiols react much slower than GSH, the major thiol compound in the cytosol, and are supposed to moderately interfere [53]. However, reduction processes are active on both the nitroxide and the biradical. Even though thiols do not reduce nitroxide directly, they increase ascorbate-induced nitroxide reduction [35,54]. Reduction potential of the tissues must be taken into account because it contributes to modification of the EPR spectrum and highly complicates the extraction of kinetic rates [51]. Once again, reduction-resistant nitroxide probes would afford an easier interpretation of in vivo observations.
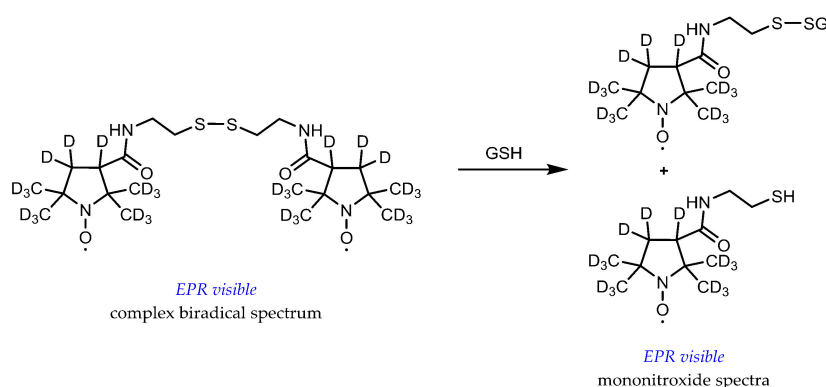
Figure 7. Principle of disulfide-linked dinitroxide spin probes for glutathione redox status evaluation.

3.2. Metabolic Biostability and Pharmacokinetics

Following in vivo administration of a nitroxide radical, the decrease of the EPR signal is not only dependent on redox processes that we previously described. It also depends on the pharmacokinetics of the compound [31]. If the probe is the substrate of an efflux pump in the cell, excretion may prevent the evaluation of oxidative stress in the tissue of interest.

Metabolic pathways relevant for nitroxides are scarce, but very efficient. Most studies in this field have focused on cyclic tetramethyl-substituted nitroxides. Depending on the structure, nitroxide elimination in vivo principally occurs through renal excretion and reduction to hydroxylamine in tissues, while reduction in the blood is negligible [55–65]. Other pathways could play a minor role for some structures, such as the transformation of the six-membered ring of TEMPO, (2,2,6,6-tetramethyl-piperidin-1-yl)oxyl, to a five-membered ring by cytochrome P450 in the liver [64,66].

For acyl-protected hydroxylamines, the rate of the deacylation process is dependent on the organ and may be rather slow outside the liver and the kidney. Ex vivo, > 70% of 500 µM ACP was cleaved in liver homogenates; 35% in kidney; 8% in brain; and < 4% in lung, stomach, heart, spleen, and muscle homogenates, or blood after 10 min at 37°C [67]. Despite the large differences in local rates of hydrolysis, the free hydroxylamine was rather uniformly distributed in the body (apart from the brain) 10 min after i.v. injection of ACP, suggesting some redistribution of the hydroxylamine after hydrolysis in the liver and kidneys [67]. Detection of oxidative stress with these probes is, therefore, not limited to intracellular RONS production in the absence of an intracellular accumulation motif.

3.3. Probe Formulation

Various modes of administration of spin probes have been used in vivo (intraperitoneal, intramuscular, i.v. [31]), but i.v. injection is the most common. When the probe is hydrophilic, phosphate-buffered and saline solutions are satisfactory vehicles. However, when hydrophobicity increases, a simple formulation of the probe compatible with i.v. injection is desirable.

3.4. Biodistribution

The rather low sensitivity of L-band EPR requires that sufficient amounts of probe reach and accumulate in the tissue of interest above the limit of detection by EPR. This becomes a critical issue when the brain is the target because a complex structure, the blood-brain barrier (BBB), protects this organ from intrusion by xenobiotics. Molecules present in the bloodstream must cross this barrier either by passive diffusion or by active transport; the actual mechanism being highly dependent on the probe structure and physicochemical properties (lipophilicity, i.e., log*P* values, molecular weight, and H-bonding capacities) [68,69]. Covalent coupling of the probe to a ligand of specific receptors expressed at the cellular membrane of the organ or tissue may help targeting. In the case of localized tumors, the probe is injected directly inside the tumor to circumvent the distribution problem.

Besides, when the EPR signal appears after reaction of the probe with RONS, it may be a problem if the probe then diffuses away from the site of RONS production. Therefore, substituents that enhance probe retention inside cells could help in better localization of oxidative stress. Introduction of esterase-clivable functionalities on carboxylic acid and phosphoric acid derivatives has been tested for this purpose [70–72]. The starting compound is cell-permeant, but a charged group is unmasked at a physiological pH after hydrolysis by intracellular esterases, which can no longer diffuse out to the extracellular space.

3.5. Spectral Properties

Usually, a spatial resolution of a few millimeters of EPR images is enough for oxidative stress mapping. It allows the distinction of different hemispheres or substructures in the brain, for instance. All other parameters being constant, the EPR imaging resolution increases with the intensity of the magnetic field gradient and decreases when the EPR linewidth of the signal (ΔH_{pp}) increases (Figure 8; the reader is referred to the appendix of reference [73] for a concise theoretical background of EPR imaging and of the influence of EPR linewidth on image resolution). The EPR linewidth must therefore be as small as possible. Typical linewidths for tetramethyl-substituted nitroxides are about 0.1 mT, which is compatible with the target image resolution. However, the linewidth is sensitive to the structure [74,75]. The major contribution to line broadening comes from unresolved hydrogen hyperfine couplings. Perdeuterated nitroxide analogues show significantly smaller linewidths than nitroxides with a natural distribution of isotopes. With piperidine nitroxides, the substitution at position four of the ring has a major influence on the linewidth. When the carbon at position four is trigonal planar, as in TEMPONE, (4-oxo-2,2,6,6-tetramethyl-piperidin-1-yl)oxyl, the conformational interchange is fast enough to allow the dynamic averaging of hyperfine couplings of hydrogens on equatorial and axial methyl groups, which results in smaller hyperfine splitting and smaller ΔH_{pp}. Substitution of the same carbon by a hydroxyl group in TEMPOL, i.e., radical (4-hydroxy-2,2,6,6-tetramethyl-piperidin-1-yl)oxyl, slows down the above-mentioned conformational interchange and results in line broadening. The replacement of methyl groups flanking the aminoxyl function with ethyl groups gives rise to additional hyperfine coupling with hydrogen and consequent line broadening with all types of rings. Bulky substituents may further increase the rotational correlation time and increase ΔH_{pp}.
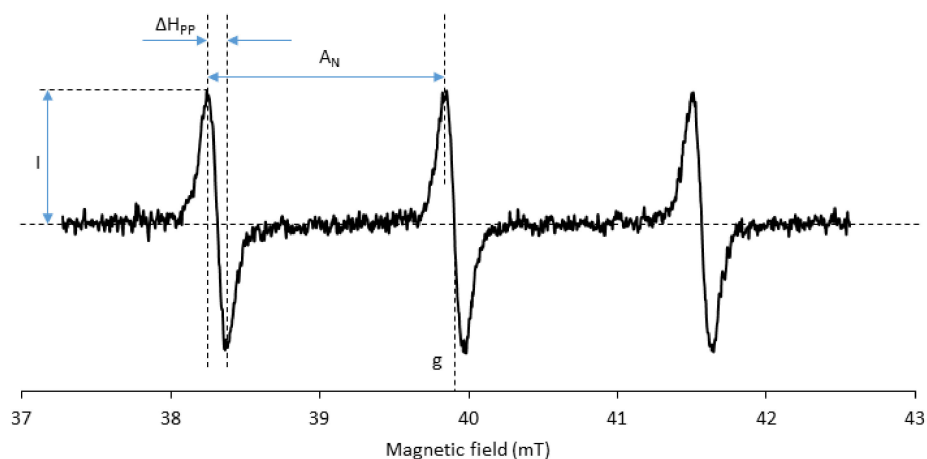
Figure 8. A typical L-band EPR spectrum of a ^{14}N-nitroxide radical in aqueous solution at 21°C; g—g factor; A_N—hyperfine coupling constant to nitrogen; ΔH_{PP}—linewidth; I—signal intensity.

Another important (and tightly linked to linewidth) parameter is the signal-to-noise ratio obtained in vivo. Indeed, the lower the signal-to-noise ratio is, the longer the image acquisition and the lower the temporal resolution of the method. An increase in the signal-to-noise ratio can be obtained by increasing the amount of probe, provided it is not toxic.

At similar injected doses, a higher signal-to-noise ratio will be obtained with a ^{15}N-labeled probe ($I = \frac{1}{2}$, two-line EPR spectrum) than with the ^{14}N-analogue ($I = 1$, three lines). Exhaustive substitution of hydrogen atoms in close vicinity to the radical center by deuterium also increases the signal-to-noise ratio. However, the relatively high cost of these isotopically substituted molecules limits their use for in vivo studies when large amounts of probes are required. Only the most promising probe candidates are usually prepared in their ^{15}N- and ^{2}H-labeled versions.

3.6. Toxicity

Typical i.v. injection doses up to 2 mmol kg^{-1} have been used for both EPR spectroscopy and imaging in rodents, even if most studies use less probe. This has to be compared to the acute LD50 of nitroxides, which is above 15 mmol kg^{-1} for (3-carboxy-2,2,5,5-tetramethylpyrrolidin-1-yl)oxyl radical **1** (Figure 9) [76], but is as low as 6 μmol kg^{-1} for TEMPOL in rats. A hypotensive effect has to be taken into account at high doses for compounds that easily permeate cell membranes and are efficient SOD-mimics, like TEMPOL [77].
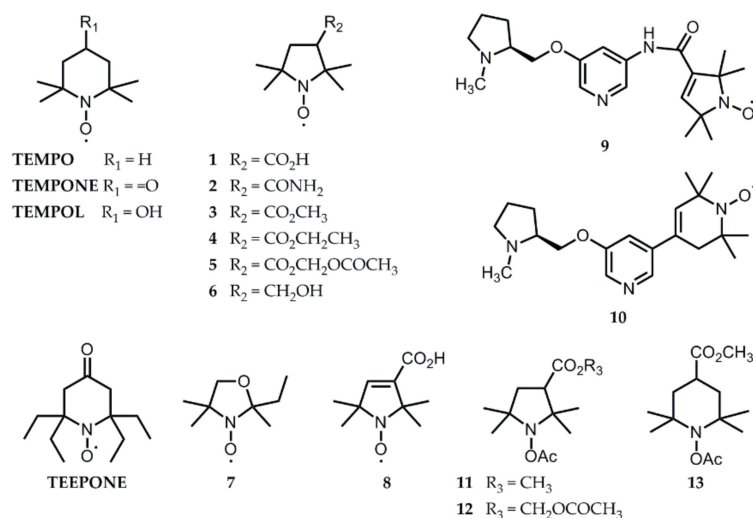
Figure 9. Structures of nitroxide and acyl-protected hydroxylamine probes mentioned in this review.

4. Solutions from the Literature That Have Already Been Tested In Vivo

4.1. Liver, Kidney, and Stomach

Nitroxide radicals are metabolized in the liver and excreted in the kidney. Their concentration is rather high in these organs. After an injection of 0.75 mmol kg^{-1} of TEMPOL in mice, the maximum nitroxide concentrations (derived from MRI measurements) in the liver and in the kidney were 1.6 and 5.3 mM, respectively [78]. Under the same conditions, 4.7 and 7.1 mM were detected for nitroxide **2**, respectively.

TEMPOL, a six-membered ring nitroxide, is too rapidly reduced to allow imaging, but it has been used to monitor reduced renal reducing activity in puromycin aminonucleoside (PAN)-induced nephrosis [62,79]. The TEMPOL EPR signal decayed slower in the kidneys of treated rats, which was linked to mitochondrial impairment using ex vivo studies. To verify the implication of RONS in this model, the acyl-protected hydroxylamine ACP was used and showed an increased nitroxide signal in the kidney only one hour after PAN administration, which was inhibited by pre-treatment with SOD, catalase, or DMSO [80]. The concentration of nitroxide formed from ACP in the kidney was estimated to be 8 μM after a 0.4 mmol kg^{-1} tail vein injection, which was too low to perform imaging.

Using water-soluble nitroxide **2** (3-carbamoyl-2,2,5,5-tetramethylpyrrolidin-1-yl)oxyl along with specially designed resonators, the liver and kidney were among the first organs to give in vivo EPR images [81–83]. At the time, EPR imaging was still invasive and minor surgery was performed to expose the target organs. In a model of streptozotocin-induced diabetic mice, the nitroxide probe was reduced faster in the diabetic kidney than in the control, an effect suppressed by Tiron (4,5-dihydroxy-1,3-benzenedisulfonate), a radical scavenger [83]. On the contrary, in Nrf2 transcriptional factor-deficient mice, a model of lupus-like autoimmune nephritis, a decrease in the reducing activity of the liver and kidney in the aged and juvenile Nrf2-deficient mice translated into a prolonged half-life of nitroxide **2** [82].

The enhanced reduction of radical **2** in tumors was used to visualize gastric carcinoma in a rat model [7]. The stomach was externalized by laparotomy for better positioning of the resonator. Normal stomach mucosa and walls exhibited a uniform distribution of the nitroxide, while the gastric tumor was clearly visible as a hole in the image.

Aiming at less invasiveness, most EPR studies of oxidative stress in vivo have been focused on the brain and hind limb of mice. The main advantage of such models is the ease of immobilization of these body parts. Indeed, compensation of contractile heart motion and animal breathing movements is still challenging in EPR imaging [84,85]. Only rare examples of the in vivo evaluation of the whole-body organ-specific redox state exist, such as EPR/MRI co-imaging of smoke-exposed mice [86].

4.2. Brain Studies

Brain studies by EPR using nitroxide radicals started in the late 1990s [87,88]. They compared the distribution in rodent head tissues of hydrophilic commercially-available structures that hardly cross the BBB, such as compound **1** (log$P$ = -1.70 [14,89]) and **2** (log$P$ = -0.26 [90]), and more lipophilic structures **3** (log$P$ = 0.94 [14,89]), **4** (log$P$ = 0.61 [89]), and **7** (log$P$ =1.04 [89]) that cross the BBB and that were synthesized for this purpose (Figure 9) [89,91,92]. Because the hyperfine coupling constant to nitrogen (A_N, Figure 8) increases with the lipophilicity of its environment, two overlapping triplet components in the spectra demonstrated partitioning of the lipophilic probes **3**, **4**, and **7** between the brain lipids and the cytosol. We can expect that redox processes would impact these two components differently, but EPR imaging is not yet able to individually record their evolution.

These lipophilic drugs are quickly eliminated from the brain by passive diffusion. To increase accumulation in the brain, Utsumi et al. [89] proposed an acetoxymethoxy ester derivative **5** (Figure 9) [89,91]. The latter is lipophilic enough (log$P$ = 0.61 [89]) to cross cell membranes and is hydrolyzed within cells by esterases to compound **1** that is trapped by the lipid bilayer thanks to its negative charge at a physiological pH. Knowing the structure of BBB, one can, however, question the localization of the nitroxide once the ester

has been cleaved. The authors stated that the probe crosses the BBB and accumulates in the brain because they detected more probe in brain tissue after oxidation by ferricyanide ex vivo. However, the probe could have been trapped within the endothelial cells lining the blood vessels, away from the brain parenchyma. The resolution of the EPR image is far too low to answer this question.

Another problem appears. According to good practice guidelines for the administration of substances in animal experimentation [93], the maximal i.v. bolus volume for rodents is 5 ml kg^{-1}. To reach 1-2 mmol kg^{-1} doses, the probe concentration in typical injections must be 200-400 mM. BBB-permeant drugs are more lipophilic and cannot be prepared in saline as a vehicle at such high concentrations. To make the stock solutions stable, the probes are often first dissolved in ethanol or methanol, and then further diluted in saline before injection (usually 10% alcohol final content is used [89]). The neurotoxicity of the vehicle is not mentioned in the articles, but it may explain why animals are sacrificed shortly after the experiment.

Later, the water-soluble and BBB-permeant probe **6** was proposed ($\log P$ = 0.26 [14]) [94] (Figure 9) and extensively used to study the effects of neuroleptics [95] and models of ischemia-reperfusion injury [12,20] or sepsis [14]. In 2014, the use of a fast EPR imager able to record one tridimensional image per minute showed, however, that the rate of EPR signal decay of nitroxide **6** in the brain is highly influenced by efflux processes, whereas for compound **3**, redox mechanisms dominate [96]. Thus, compound **6** would not be a reliable reporter of redox processes in the brain. The apparent half-life of radical **3** in the brain is extremely short ($t_{1/2}$ = 2-3 min), and it cannot be recorded with current commercially-available spectrometers. Compound **3** is now the most currently used nitroxide probe for oxidative stress imaging using fast new generation EPR imagers and has been tested in a large variety of animal models (epilepsy, Alzheimer's disease, methamphetamine-induced dopaminergic neurotoxicity) [17,97–101]. Interestingly, some of these studies showed an enhanced rate of EPR signal decrease in the pathological situation [97,100,101] and this was interpreted as a sign of oxidative damage, whereas other studies using the same EPR probe showed a prolonged half-life of nitroxide **3** in the sick brain and assigned it to a decrease in the reducing abilities of selected brain regions [17,36,98]. The direction of variations was opposite in two mouse models of Alzheimer's disease [98,99]. In the more recent studies, efforts were made to correlate the results obtained by EPR imaging with other techniques: biochemical assays for GSH, cysteine, and ascorbate levels [17,97]; SOD activity [98]; or lipid peroxidation [97], immunohistochemistry [98], or MRI evaluation of BBB function [97]. Even with these correlations, it is not always possible to unambiguously track down the origin of enhanced nitroxide reduction. In methamphetamine-treated mice, both elevated RONS and the inhibition of cytochrome c oxidase (complex IV in the mitochondrial respiratory chain, which is known to reoxidize lipophilic hydroxylamines [49]) could explain enhanced nitroxide decay, and it was not related to variations in GSH levels or GSH redox status [97]. It is thus highly controversial to universally use redox maps obtained from EPR imaging of nitroxide **3** to estimate GSH levels, as recently proposed by Emoto et al. [100,101].

In an attempt to increase the stability of nitroxides towards biological reduction and thus to make them compatible with current commercial EPR imagers, synthetic efforts have been focused on tuning the steric and electronic environment of the aminoxyl function. The introduction of four ethyl groups effectively protects against reduction by ascorbate in vitro [102,103]. It is likely to also afford protection against reductases and mono-oxygenases, thereby increasing the selectivity of measurement, but this has never been verified, to our knowledge. Radical 4-oxo-2,2,6,6-tetraethyl-piperidin-1-yl)oxyl (TEEPONE, Figure 9) and its ^{15}N analogue displayed an apparent half-life above 80 minutes in the mouse brain in vivo [104]. However, the lipophilic character is even higher in these structures ($\log P$ = 2.14 [90]) and the formulation of the probe becomes a key issue. Different unsuccessful trials have been made using liposome and cyclodextrin encapsulation. Dissolution of TEEPONE in a lipophilic emulsion designed for human parenteral nutrition (10% INTRAFAT) gave satisfactory results for both EPR and MRI imaging in control animals, but has not been tested in pathological models [104,105]. Even if this formulation opens interesting perspectives, the use of a pre-formed

emulsion as a vehicle may not be universal. Crystalline compounds, such as nitroxide **5**, for instance, do not significantly dissolve in this emulsion. The development of tailored formulations thus appears as a future important aspect of the development of probes for EPR imaging.

Conjugation of nitroxide probes with a ligand of nicotine acetylcholine receptors, mainly localized in the central and peripheral nervous systems, was tested with compounds **9** and **10** as a tool for targeted delivery of the EPR probe to the brain (Figure 9) [106]. Compound **10** demonstrated enhanced and specific accumulation in the brain in opposition to compound **6**, which distributed in all head tissues and to compound **8**, which was excluded from the brain due to its negative charge at a physiological pH. Compound **9**, despite its very close structure, was totally BBB-impermeant. While they did not report on the log*P* values of compounds **9** and **10**, the authors attributed this differential behavior to the presence of an amide linkage with an H-bonding capacity in compound **9**. Unfortunately, the potential neurotoxicity of compound **10** is a limitation to further use of this probe for longitudinal studies.

Acyl-protected hydroxylamine probes were also tested as brain imaging agents. In a rat model of kainic acid (KA)-induced epileptic seizures, a 5 mmol kg^{-1} intraperitoneal injection of ACP allowed EPR imaging and revealed a greater EPR signal intensity in the hippocampus and striatum in the KA group versus control, while intensities in the cortex were similar [43]. This effect was not due to differences in ACP uptake between groups or regions of the brain. The observations correlated with higher lipid radical levels in the hippocampus of KA-treated rats and were thus attributed to enhanced RONS production in selected brain regions. Searching for acyl-protected hydroxylamines with higher BBB-penetration, a series of lipophilic compounds **11**-**13** were synthesized (Figure 9; log*P* not reported), and their biodistribution was assessed in vivo [44]. While compounds **12** and **13** were hardly detected in the brain, compound **11** was shown as a promising candidate, but has never been used since then.

4.3. Hind Limb-Implanted Tumor Studies

Cell-permeant nitroxides allow the EPR evaluation of intracellular tumor reducing capacity. Compound **2** has been used since the late 1990s in the mouse radiation-induced fibrosarcoma (RIF-1) tumor model to image nitroxide distribution and bioreduction heterogeneity in tumor tissue [5]. The exchange interaction between molecular oxygen and nitroxide modulates the EPR linewidth of the nitroxide from which the tissue oxygen content can be derived. Perdeuterated-TEMPONE was then used as an oximetry probe, before being replaced with more sensitive probes, such as particulate lithium phthalocyanine spin probes or trityl radicals [107]. Compound **6** was later used in the same model as a redox-sensitive probe [9].

In recent years, major efforts have been dedicated to the development of extracellular dual probes for redox and pH, such as that displayed in Figure 10 [10,108], and of probes for GSH redox status (Figure 7) [51,52]. A multifunctional approach is indeed crucial for understanding tumor physiology and metabolism.
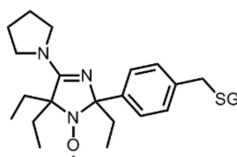

Figure 10. A typical dual pH-redox nitroxide probe for investigation of the tumor microenvironment. Covalent linkage to a charged glutathione moiety (-SG group in the structure) ensures extracellular localization and prevents diffusion through cell membranes. The ethyl groups close to the redox-sensitive nitroxide function enhance nitroxide stability towards reduction, affording a slow enough reduction rate (t$_{1/2}$ ≈ 5 min) for monitoring the reducing capacity of the extracellular matrix of the tumor. Protonation of the N-3 atom induces a strong variation (≈ 0.1 mT) in the hyperfine splitting A$_N$, which is used as a pH-sensitive marker. The pKa of the probe (6.60 at 37°C) has been tuned for the measurement of extracellular tumor acidity through the introduction of a pyrrolidine substituent at position 4 of the imidazoline ring.

5. Perspectives from In Vitro Results

Progress towards in vivo imaging of cyclic nitrone spin adducts has recently been made using rapid-scan EPR and improved algorithms for image reconstruction [109]. We may thus hope that spin traps will become applicable for the in vivo identification of radicals in the near future. However, quantification of radical production using spin traps is likely to remain difficult because of competition with the biological elimination processes and because the reduction processes may vary from one biological condition to the other.

Besides, trityl-based probes are currently being developed as selective and quantitative sensors for superoxides, but have not yet been tested in vivo [110,111]. Their selectivity relies on the specific transformation of tetrathiatriarylmethyl radicals by a superoxide to quinone-methide products [112] (Figure 11). Their narrow EPR linewidth ($\approx$0.02 mT under anaerobic conditions) makes them very promising probes for imaging. Dendritic encapsulation enhances the selectivity for a superoxide and increases the resistance against reduction to the corresponding triarylmethanes, while only moderately decreasing the reaction rate with a superoxide (k $\approx 10^4$ M^{-1} s^{-1}) and reducing albumin binding [110]. These sensors are, however, not able to permeate cells and will thus be limited to extracellular detection of a superoxide. Moreover, the prohibitive cost of trityl-based probes may prevent a widespread use in vivo.
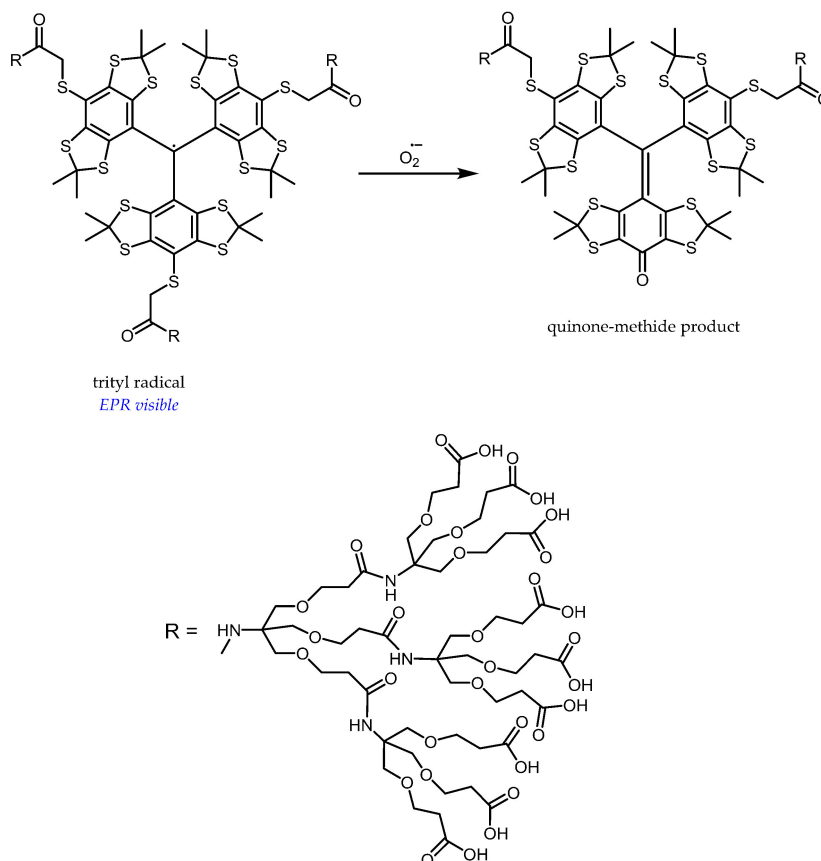
Figure 11. Principle of dendritic trityl-based selective sensors for a superoxide.

In vitro, selectivity for oxidative processes has also been obtained with imidazolidine nitroxides substituted by four ethyl groups at the alpha positions of the aminoxyl function and bearing a hydrogen atom at position four of the heterocycle (Figure 12). These radicals are resistant to reduction and undergo irreversible oxidative fragmentation in the presence of mono-electronic oxidants [113]. Imidazolidine nitroxides bearing four geminal ethyl groups show rather large linewidths ($\approx$0.7 mT),

notably due to the hindered rotation of ethyl groups by substituents at position three and four of the ring [114,115]. Deuteration would therefore be required prior to in vivo application.
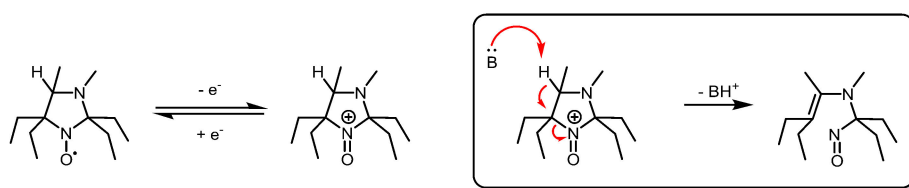
Figure 12. Imidazolidine nitroxides bearing a hydrogen atom at position four of the heterocycle are oxidized to unstable oxoammonium cations by monoelectronic oxidants (superoxide, peroxyl, or lipid-derived radicals). Proton abstraction by a weak base (B) induces irreversible ring fragmentation.

6. Conclusions

Continued progress in EPR spectroscopy and imaging has made the investigation of in vivo oxidative stress more and more accessible. A better understanding of probe reactivity and pharmacokinetics, together with the parameters that control EPR spectroscopic properties, has been obtained. However, we are still searching for the ideal probe that would combine all the knowledge acquired over the years. Great care should be taken in interpretation of the results and the complementary use of additional techniques will help to unravel the origin of oxidative stress.

Abbreviations

ACP—1-acetoxy-3-carbamoyl-2,2,5,5- tetramethylpyrrolidine;
ALS—amyotrophic lateral sclerosis;
A_N—hyperfine coupling constant to nitrogen;
BBB—blood-brain barrier;
BMPO—5-tert-butoxycarbonyl-5-methyl-1-pyrroline N-oxide;
CMH—1-hydroxy-3-methoxycarbonyl-2,2,5,5-tetramethylpyrrolidine;
CW—continuous wave;
ΔH_{pp}—EPR peak-to-peak linewidth;
DEPMPO—5-diethoxyphosphoryl-5-methyl-1-pyrroline N-oxide;
DETC—diethyldithiocarbamate;
DMPO—5,5-dimethyl-1-pyrroline *N*-oxide;
DMSO—dimethyl sulfoxide;
DTCS—N-(dithiocarboxy)sarcosine;
EPR—electron paramagnetic resonance;
GSH—glutathione;
GSSG—glutathione disulfide;
i.v.—intravenous;
KA—kainic acid;
L-Arg—L-arginine;
L-Cit—L-citrulline;
L-NAME—N(ω)-nitro-L-arginine methyl ester;
log*P*—$\log_{10}$ of the octanol-water partition coefficient;
LPS—lipopolysaccharide;
MAO—monoamine-oxidases;
MGD—N-methyl-D-glucamine dithiocarbamate;
MRI—magnetic resonance imaging;
NAD(P)H—nicotinamide adenine dinucleotide (phosphate);
NOS—nitric oxide synthase;
PAN—puromycin aminonucleoside;
RIF-1—radiation-induced fibrosarcoma;
RONS—reactive oxygen and nitrogen species;
SOD—superoxide dismutase;
TEEPONE—4-oxo-2,2,6,6-tetraethyl-piperidin-1-yl)oxyl;
TEMPO—(2,2,6,6-tetramethyl-piperidin-1-yl)oxyl;
TEMPOL—4-hydroxy-2,2,6,6-tetramethyl-piperidin-1-yl)oxyl;
TEMPONE—(4-oxo-2,2,6,6-tetramethyl-piperidin-1-yl)oxyl;
Tiron—4,5-dihydroxy-1,3-benzenedisulfonate.

References

1. Sies, H. Oxidative stress: A concept in redox biology and medicine. *Redox Biol.* **2015**, *4*, 180–183. [CrossRef] [PubMed]

2. Swartz, H.M.; Williams, B.B.; Zaki, B.I.; Hartford, A.C.; Jarvis, L.A.; Chen, E.Y.; Comi, R.J.; Ernstoff, M.S.; Hou, H.; Khan, N.; et al. Clinical EPR: Unique opportunities and some challenges. *Acad. Radiol.* **2014**, *21*, 197–206. [CrossRef] [PubMed]

3. Epel, B.; Redler, G.; Tormyshev, V.; Halpern, H.J. Towards human oxygen images with electron paramagnetic resonance imaging. *Adv. Exp. Med. Biol.* **2016**, *876*, 363–369. [PubMed]

4. Elas, M.; Ichikawa, K.; Halpern, H.J. Oxidative stress imaging in live animals with techniques based on electron paramagnetic resonance. *Radiat. Res.* **2012**, *177*, 514–523. [CrossRef] [PubMed]

5. Kuppusamy, P.; Afeworki, M.; Shankar, R.A.; Coffin, D.; Krishna, M.C.; Hahn, S.M.; Mitchell, J.B.; Zweier, J.L. In vivo electron paramagnetic resonance imaging of tumor heterogeneity and oxygenation in a murine model. *Cancer Res.* **1998**, *58*, 1562–1568. [PubMed]

6. Kuppusamy, P.; Li, H.; Ilangovan, G.; Cardounel, A.J.; Zweier, J.L.; Yamada, K.; Krishna, M.C.; Mitchell, J.B. Noninvasive imaging of tumor redox status and its modification by tissue glutathione levels. *Cancer Res.* **2002**, *62*, 307–312. [PubMed]

7. Mikuni, T.; He, G.; Petryakov, S.; Fallouh, M.M.; Deng, Y.; Ishihara, R.; Kuppusamy, P.; Tatsuta, M.; Zweier, J.L. In vivo detection of gastric cancer in rats by electron paramagnetic resonance imaging. *Cancer Res.* **2004**, *64*, 6495–6502. [CrossRef]

8. Hyodo, F.; Matsumoto, K.-I.; Matsumoto, A.; Mitchell, J.B.; Krishna, M.C. Probing the intracellular redox status of tumors with magnetic resonance imaging and redox-sensitive contrast agents. *Cancer Res.* **2006**, *66*, 9921–9928. [CrossRef]

9. Takeshita, K.; Kawaguchi, K.; Fujii-Aikawa, K.; Ueno, M.; Okazaki, S.; Ono, M.; Krishna, M.C.; Kuppusamy, P.; Ozawa, T.; Ikota, N. Heterogeneity of regional redox status and relation of the redox status to oxygenation in a tumor model, evaluated using electron paramagnetic resonance imaging. *Cancer Res.* **2010**, *70*, 4133–4140. [CrossRef]

10. Bobko, A.A.; Eubank, T.D.; Voorhees, J.L.; Efimova, O.V.; Kirilyuk, I.A.; Petryakov, S.; Trofimiov, D.G.; Marsh, C.B.; Zweier, J.L.; Grigor'ev, I.A.; et al. In vivo monitoring of pH, redox status, and glutathione using L-band EPR for assessment of therapeutic effectiveness in solid tumors. *Magn. Reson. Med.* **2012**, *67*, 1827–1836. [CrossRef]

11. Yamato, M.; Egashira, T.; Utsumi, H. Application of in vivo ESR spectroscopy to measurement of cerebrovascular ROS generation in stroke. *Free Radic. Biol. Med.* **2003**, *35*, 1619–1631. [CrossRef] [PubMed]

12. Yokoyama, H.; Ueda, Y.; Itoh, O.; Ikeda, T.; Noor, J.I.; Ikenoue, T. EPR imaging to estimate the in vivo intracerebral reducing ability of mature rats after neonatal hypoxic-ischemic brain injury. *Magn. Reson. Imaging* **2004**, *22*, 1305–1309. [CrossRef] [PubMed]

13. Hyodo, F.; Chuang, K.-H.; Goloshevsky, A.G.; Sulima, A.; Griffiths, G.L.; Mitchell, J.B.; Koretsky, A.P.; Krishna, M.C. Brain redox imaging using blood-brain barrier-permeable nitroxide MRI contrast agent. *J. Cereb. Blood Flow Metab. Off. J. Int. Soc. Cereb. Blood Flow Metab.* **2008**, *28*, 1165–1174. [CrossRef] [PubMed]

14. Fujii, H.G.; Sato-Akaba, H.; Emoto, M.C.; Itoh, K.; Ishihara, Y.; Hirata, H. Noninvasive mapping of the redox status in septic mouse by in vivo electron paramagnetic resonance imaging. *Magn. Reson. Imaging* **2013**, *31*, 130–138. [CrossRef] [PubMed]

15. Lee, M.-C.-I. Assessment of oxidative stress and antioxidant property using electron spin resonance (ESR) spectroscopy. *J. Clin. Biochem. Nutr.* **2013**, *52*, 1–8. [CrossRef] [PubMed]

16. Okazaki, S.; Tachibana, Y.; Koga-Ogawa, Y.; Takeshita, K. Redox evaluation in sepsis model mice by the in vivo ESR technique using acyl-protected hydroxylamine. *Free Radic. Biol. Med.* **2014**, *68*, 72–79. [CrossRef] [PubMed]

17. Emoto, M.C.; Yamato, M.; Sato-Akaba, H.; Yamada, K.; Fujii, H.G. Brain redox imaging in the pentylenetetrazole (PTZ)-induced kindling model of epilepsy by using in vivo electron paramagnetic resonance and a nitroxide imaging probe. *Neurosci. Lett.* **2015**, *608*, 40–44. [CrossRef] [PubMed]

18. Hyodo, F.; Matsumoto, S.; Devasahayam, N.; Dharmaraj, C.; Subramanian, S.; Mitchell, J.B.; Krishna, M.C. Pulsed EPR imaging of nitroxides in mice. *J. Magn. Reson.* **2009**, *197*, 181–185. [CrossRef]

19. Eaton, S.S.; Shi, Y.; Woodcock, L.; Buchanan, L.A.; McPeak, J.; Quine, R.W.; Rinard, G.A.; Epel, B.; Halpern, H.J.; Eaton, G.R. Rapid-scan EPR imaging. *J. Magn. Reson.* **2017**, *280*, 140–148. [CrossRef]

20. Fujii, H.; Sato-Akaba, H.; Kawanishi, K.; Hirata, H. Mapping of redox status in a brain-disease mouse model by three-dimensional EPR imaging. *Magn. Reson. Med.* **2011**, *65*, 295–303. [CrossRef]

21. Ahmad, R.; Samouilov, A.; Zweier, J.L. Accelerated dynamic EPR imaging using fast acquisition and compressive recovery. *J. Magn. Reson.* **2016**, *273*, 105–112. [CrossRef] [PubMed]

22. Komarov, D.A.; Hirata, H. Fast backprojection-based reconstruction of spectral-spatial EPR images from projections with the constant sweep of a magnetic field. *J. Magn. Reson.* **2017**, *281*, 44–50. [CrossRef]

23. Halpern, H.J.; Yu, C.; Barth, E.; Peric, M.; Rosen, G.M. In situ detection, by spin trapping, of hydroxyl radical markers produced from ionizing radiation in the tumor of a living mouse. *Proc. Natl. Acad. Sci. USA* **1995**, *92*, 796–800. [CrossRef] [PubMed]

24. Pignitter, M.; Gorren, A.C.F.; Nedeianu, S.; Schmidt, K.; Mayer, B. Inefficient spin trapping of superoxide in the presence of nitric-oxide: Implications for studies on nitric-oxide synthase uncoupling. *Free Radic. Biol. Med.* **2006**, *41*, 455–463. [CrossRef] [PubMed]

25. Lauricella, R.P.; Bouteiller, J.-C.H.; Tuccio, B.N. Evidence of overestimation of rate constants for the superoxide trapping by nitrones in aqueous media. *Phys. Chem. Chem. Phys.* **2005**, *7*, 399–404. [CrossRef] [PubMed]

26. Bézière, N.; Frapart, Y.; Rockenbauer, A.; Boucher, J.-L.; Mansuy, D.; Peyrot, F. Metabolic stability of superoxide and hydroxyl radical adducts of a cyclic nitrone toward rat liver microsomes and cytosol: A stopped-flow ESR spectroscopy study. *Free Radic. Biol. Med.* **2010**, *49*, 437–446. [CrossRef] [PubMed]

27. Bézière, N.; Hardy, M.; Poulhès, F.; Karoui, H.; Tordo, P.; Ouari, O.; Frapart, Y.-M.; Rockenbauer, A.; Boucher, J.-L.; Mansuy, D.; et al. Metabolic stability of superoxide adducts derived from newly developed cyclic nitrone spin traps. *Free Radic. Biol. Med.* **2014**, *67*, 150–158. [CrossRef]

28. Nagano, T.; Yoshimura, T. Bioimaging of Nitric Oxide. *Chem. Rev.* **2002**, *102*, 1235–1270. [CrossRef]

29. Hong, H.; Sun, J.; Cai, W. Multimodality imaging of nitric oxide and nitric oxide synthases. *Free Radic. Biol. Med.* **2009**, *47*, 684–698. [CrossRef]

30. Kocherginsky, N.; Swartz, H.M. *Nitroxide Spin Labels: Reactions in Biology and Chemistry*; CRC Press: Boca Raton, FL, USA, 1995; ISBN 978-0-8493-4204-2.

31. Bačić, G.; Pavićević, A.; Peyrot, F. In vivo evaluation of different alterations of redox status by studying pharmacokinetics of nitroxides using magnetic resonance techniques. *Redox Biol.* **2016**, *8*, 226–242. [CrossRef]

32. Giotta, G.J.; Wang, H.H. Reduction of nitroxide free radicals by biological materials. *Biochem. Biophys. Res. Commun.* **1972**, *46*, 1576–1580. [CrossRef]

33. Chen, K.; Swartz, H.M. The products of the reduction of doxyl stearates in cells are hydroxylamines as shown by oxidation by 15N-perdeuterated Tempone. *Biochim. Biophys. Acta* **1989**, *992*, 131–133. [CrossRef]

34. Swartz, H.M. Principles of the metabolism of nitroxides and their implications for spin trapping. *Free Radic. Res. Commun.* **1990**, *9*, 399–405. [CrossRef]

35. Bobko, A.A.; Kirilyuk, I.A.; Grigor'ev, I.A.; Zweier, J.L.; Khramtsov, V.V. Reversible reduction of nitroxides to hydroxylamines: Roles for ascorbate and glutathione. *Free Radic. Biol. Med.* **2007**, *42*, 404–412. [CrossRef] [PubMed]

36. Yokoyama, H.; Itoh, O.; Ohya-Nishiguchi, H.; Kamada, H. Reducing ability of the striatum and cerebral cortex in rats following acute administration of risperidone or haloperidol: An estimation by in vivo electron paramagnetic resonance imaging. *Neurochem. Res.* **2002**, *27*, 243–248. [CrossRef] [PubMed]

37. Krishna, M.; Grahame, D.; Samuni, A.; Mitchell, J.; Russo, A. Oxoammonium cation intermediate in the nitroxide-catalyzed dismutation. *Proc. Natl. Acad. Sci. USA* **1992**, *89*, 5537–5541. [CrossRef] [PubMed]

38. Goldstein, S.; Samuni, A.; Hideg, K.; Merenyi, G. Structure-activity relationship of cyclic nitroxides as SOD mimics and scavengers of nitrogen dioxide and carbonate radicals. *J. Phys. Chem. A* **2006**, *110*, 3679–3685. [CrossRef]

39. Goldstein, S.; Samuni, A.; Russo, A. Reaction of cyclic nitroxides with nitrogen dioxide: The intermediacy of the oxoammonium cations. *J. Am. Chem. Soc.* **2003**, *125*, 8364–8370. [CrossRef]

40. Goldstein, S.; Samuni, A.; Merenyi, G. Reactions of nitric oxide, peroxynitrite, and carbonate radicals with nitroxides and their corresponding oxoammonium cations. *Chem. Res. Toxicol.* **2004**, *17*, 250–257. [CrossRef]

41. Goldstein, S.; Merenyi, G.; Russo, A.; Samuni, A. The role of oxoammonium cation in the SOD-mimic activity of cyclic nitroxides. *J. Am. Chem. Soc.* **2003**, *125*, 789–795. [CrossRef]

42. Itoh, O.; Aoyama, M.; Yokoyama, H.; Obara, H.; Ohya, H.; Kamada, H. Sensitive ESR determination of intracellular oxidative stress by using acyl-protected hydroxylamines as new spin reagents. *Chem. Lett.* **2000**, *4*, 304–305. [CrossRef]

43. Yokoyama, H.; Itoh, O.; Aoyama, M.; Obara, H.; Ohya, H.; Kamada, H. In vivo EPR imaging by using an acyl-protected hydroxylamine to analyze intracerebral oxidative stress in rats after epileptic seizures. *Magn. Reson. Imaging* **2000**, *18*, 875–879. [CrossRef]

44. Yordanov, A.T.; Yamada, K.; Krishna, M.C.; Russo, A.; Yoo, J.; English, S.; Mitchell, J.B.; Brechbiel, M.W. Acyl-protected hydroxylamines as spin label generators for EPR brain imaging. *J. Med. Chem.* **2002**, *45*, 2283–2288. [CrossRef] [PubMed]

45. Dikalov, S.I.; Polienko, Y.F.; Kirilyuk, I. Electron paramagnetic resonance measurements of reactive oxygen species by cyclic hydroxylamine spin probes. *Antioxid. Redox Signal.* **2018**, *28*, 1433–1443. [CrossRef] [PubMed]

46. Zhang, R.; Goldstein, S.; Samuni, A. Kinetics of superoxide-induced exchange among nitroxide antioxidants and their oxidized and reduced forms. *Free Radic. Biol. Med.* **1999**, *26*, 1245–1252. [CrossRef]

47. Griesser, M.; Shah, R.; Van Kessel, A.T.; Zilka, O.; Haidasz, E.A.; Pratt, D.A. The catalytic reaction of nitroxides with peroxyl radicals and its relevance to their cytoprotective properties. *J. Am. Chem. Soc.* **2018**, *140*, 3798–3808. [CrossRef] [PubMed]

48. Dikalov, S.; Skatchkov, M.; Bassenge, E. Quantification of peroxynitrite, superoxide, and peroxyl radicals by a new spin trap hydroxylamine 1-hydroxy-2,2,6,6-tetramethyl-4-oxo-piperidine. *Biochem. Biophys. Res. Commun.* **1997**, *230*, 54–57. [CrossRef] [PubMed]

49. Chen, K.; Swartz, H.M. Oxidation of hydroxylamines to nitroxide spin labels in living cells. *Biochim. Biophys. Acta* **1988**, *970*, 270–277. [CrossRef]

50. Giustarini, D.; Colombo, G.; Garavaglia, M.L.; Astori, E.; Portinaro, N.M.; Reggiani, F.; Badalamenti, S.; Aloisi, A.M.; Santucci, A.; Rossi, R.; et al. Assessment of glutathione/glutathione disulphide ratio and S-glutathionylated proteins in human blood, solid tissues, and cultured cells. *Free Radic. Biol. Med.* **2017**, *112*, 360–375. [CrossRef]

51. Roshchupkina, G.I.; Bobko, A.A.; Bratasz, A.; Reznikov, V.A.; Kuppusamy, P.; Khramtsov, V.V. In vivo EPR measurement of glutathione in tumor-bearing mice using improved disulfide biradical probe. *Free Radic. Biol. Med.* **2008**, *45*, 312–320. [CrossRef]

52. Epel, B.; Sundramoorthy, S.V.; Krzykawska-Serda, M.; Maggio, M.C.; Tseytlin, M.; Eaton, G.R.; Eaton, S.S.; Rosen, G.M.; Kao, J.P.Y.; Halpern, H.J. Imaging thiol redox status in murine tumors in vivo with rapid-scan electron paramagnetic resonance. *J. Magn. Reson.* **2017**, *276*, 31–36. [CrossRef] [PubMed]

53. Khramtsov, V.V.; Yelinova, V.I.; Glazachev, Y.; Reznikov, V.A.; Zimmer, G. Quantitative determination and reversible modification of thiols using imidazolidine biradical disulfide label. *J. Biochem. Biophys. Methods* **1997**, *35*, 115–128. [CrossRef]

54. Chen, K.Y.; McLaughlin, M.G. Differences in the reduction kinetics of incorporated spin labels in undifferentiated and differentiated mouse neuroblastoma cells. *Biochim. Biophys. Acta* **1985**, *845*, 189–195. [CrossRef]

55. Couet, W.R.; Eriksson, U.G.; Tozer, T.N.; Tuck, L.D.; Wesbey, G.E.; Nitecki, D.; Brasch, R.C. Pharmacokinetics and metabolic fate of two nitroxides potentially useful as contrast agents for magnetic resonance imaging. *Pharm. Res.* **1984**, *1*, 203–209. [CrossRef] [PubMed]

56. Bacic, G.; Nilges, M.J.; Magin, R.L.; Walczak, T.; Swartz, H.M. In vivo localized ESR spectroscopy reflecting metabolism. *Magn. Reson. Med.* **1989**, *10*, 266–272. [CrossRef] [PubMed]

57. Utsumi, H.; Muto, E.; Masuda, S.; Hamada, A. In vivo ESR measurement of free radicals in whole mice. *Biochem. Biophys. Res. Commun.* **1990**, *172*, 1342–1348. [CrossRef]

58. Miura, Y.; Utsumi, H.; Hamada, A. Effects of inspired oxygen concentration on in vivo redox reaction of nitroxide radicals in whole mice. *Biochem. Biophys. Res. Commun.* **1992**, *182*, 1108–1114. [CrossRef]

59. Vianello, F.; Momo, F.; Scarpa, M.; Rigo, A. Kinetics of nitroxide spin label removal in biological systems: An in vitro and in vivo ESR study. *Magn. Reson. Imaging* **1995**, *13*, 219–226. [CrossRef]

60. Seimenis, I.; Foster, M.A.; Lurie, D.J.; Hutchison, J.M.S.; Whiting, P.H.; Payne, S. The excretion mechanism of the spin label proxyl carboxylic acid (PCA) from the rat monitored by X-band ESR and PEDRI. *Magn. Reson. Med.* **1997**, *37*, 552–558. [CrossRef]

61. Kroll, C.; Borchert, H.H. Metabolism of the stable nitroxyl radical 4-oxo-2,2,6, 6-tetramethylpiperidine-N-oxyl (TEMPONE). *Eur. J. Pharm. Sci. Off. J. Eur. Fed. Pharm. Sci.* **1999**, *8*, 5–9.

62. Ueda, A.; Nagase, S.; Yokoyama, H.; Tada, M.; Noda, H.; Ohya, H.; Kamada, H.; Hirayama, A.; Koyama, A. Importance of renal mitochondria in the reduction of TEMPOL, a nitroxide radical. *Mol. Cell. Biochem.* **2003**, *244*, 119–124. [CrossRef] [PubMed]

63. Matsumoto, K.-I.; Krishna, M.C.; Mitchell, J.B. Novel pharmacokinetic measurement using electron paramagnetic resonance spectroscopy and simulation of in vivo decay of various nitroxyl spin probes in mouse blood. *J. Pharmacol. Exp. Ther.* **2004**, *310*, 1076–1083. [CrossRef] [PubMed]

64. Okajo, A.; Matsumoto, K.; Mitchell, J.B.; Krishna, M.C.; Endo, K. Competition of nitroxyl contrast agents as an in vivo tissue redox probe: Comparison of pharmacokinetics by the bile flow monitoring (BFM) and blood circulating monitoring (BCM) methods using X-band EPR and simulation of decay profiles. *Magn. Reson. Med.* **2006**, *56*, 422–431. [CrossRef] [PubMed]

65. Zhelev, Z.; Matsumoto, K.-I.; Gadjeva, V.; Bakalova, R.; Aoki, I.; Zheleva, A.; Anzai, K. EPR signal reduction kinetic of several nitroxyl derivatives in blood in vitro and in vivo. *Gen. Physiol. Biophys.* **2009**, *28*, 356–362. [CrossRef] [PubMed]

66. Yin, W.; Mitra, K.; Stearns, R.A.; Baillie, T.A.; Kumar, S. Conversion of the 2,2,6,6-tetramethylpiperidine moiety to a 2,2-dimethylpyrrolidine by cytochrome P450: Evidence for a mechanism involving nitroxide radicals and heme iron. *Biochemistry* **2004**, *43*, 5455–5466. [CrossRef] [PubMed]

67. Saito, K.; Takeshita, K.; Anzai, K.; Ozawa, T. Pharmacokinetic study of acyl-protected hydroxylamine probe, 1-acetoxy-3-carbamoyl-2,2,5,5-tetramethylpyrrolidine, for in vivo measurements of reactive oxygen species. *Free Radic. Biol. Med.* **2004**, *36*, 517–525. [CrossRef]

68. Chen, Y.; Liu, L. Modern methods for delivery of drugs across the blood-brain barrier. *Adv. Drug Deliv. Rev.* **2012**, *64*, 640–665. [CrossRef]

69. Testa, B.; Crivori, P.; Reist, M.; Carrupt, P.-A. The influence of lipophilicity on the pharmacokinetic behavior of drugs: Concepts and examples. *Perspect. Drug Discov. Des.* **2000**, *19*, 179–211. [CrossRef]

70. Sosnovsky, G.; Rao, N.; Li, S.; Swartz, H. Synthesis of nitroxyl (aminoxyl) labeled probes for studies of intracellular environment by EPR and MRI. *J. Org. Chem.* **1989**, *54*, 3667–3674. [CrossRef]

71. Hu, H.P.; Sosnovsky, G.; Li, S.W.; Rao, N.U.; Morse, P.D.; Swartz, H.M. Development of nitroxides for selective localization inside cells. *Biochim. Biophys. Acta* **1989**, *1014*, 211–218. [CrossRef]

72. Dikalov, S.I.; Dikalova, A.E.; Morozov, D.A.; Kirilyuk, I.A. Cellular accumulation and antioxidant activity of acetoxymethoxycarbonyl pyrrolidine nitroxides. *Free Radic. Res.* **2018**, *52*, 339–350. [CrossRef] [PubMed]

73. Binet, L.; Gourier, D.; Derenne, S. Potential of EPR imaging to detect traces of primitive life in sedimentary rocks. *Earth Planet. Sci. Lett.* **2008**, *273*, 359–366. [CrossRef]

74. Burks, S.R.; Makowsky, M.A.; Yaffe, Z.A.; Hoggle, C.; Tsai, P.; Muralidharan, S.; Bowman, M.K.; Kao, J.P.Y.; Rosen, G.M. The effect of structure on nitroxide EPR spectral linewidth. *J. Org. Chem.* **2010**, *75*, 4737–4741. [CrossRef] [PubMed]

75. Biller, J.R.; Meyer, V.; Elajaili, H.; Rosen, G.M.; Kao, J.P.Y.; Eaton, S.S.; Eaton, G.R. Relaxation times and line widths of isotopically-substituted nitroxides in aqueous solution at X-band. *J. Magn. Reson.* **2011**, *212*, 370–377. [CrossRef] [PubMed]

76. Afzal, V.; Brasch, R.C.; Nitecki, D.E.; Wolff, S. Nitroxyl spin label contrast enhancers for magnetic resonance imaging. Studies of acute toxicity and mutagenesis. *Investig. Radiol.* **1984**, *19*, 549–552. [CrossRef]

77. Hahn, S.M.; Sullivan, F.J.; DeLuca, A.M.; Bacher, J.D.; Liebmann, J.; Krishna, M.C.; Coffin, D.; Mitchell, J.B. Hemodynamic effect of the nitroxide superoxide dismutase mimics. *Free Radic. Biol. Med.* **1999**, *27*, 529–535. [CrossRef]

78. Davis, R.M.; Matsumoto, S.; Bernardo, M.; Sowers, A.; Matsumoto, K.-I.; Krishna, M.C.; Mitchell, J.B. Magnetic resonance imaging of organic contrast agents in mice: Capturing the whole-body redox landscape. *Free Radic. Biol. Med.* **2011**, *50*, 459–468. [CrossRef]

79. Ueda, A.; Nagase, S.; Yokoyama, H.; Tada, M.; Ohya, H.; Kamada, H.; Hirayama, A.; Koyama, A. Identification by an EPR technique of decreased mitochondrial reducing activity in puromycin aminonucleoside-induced nephrosis. *Free Radic. Biol. Med.* **2002**, *33*, 1082–1088. [CrossRef]

80. Ueda, A.; Hirayama, A.; Nagase, S.; Inoue, M.; Oteki, T.; Aoyama, M.; Yokoyama, H. In vivo detection of intrinsic reactive oxygen species using acyl-protected hydroxylamine in puromycin nephrosis. *Free Radic. Res.* **2007**, *41*, 823–828. [CrossRef]

81. Ueda, A.; Yokoyama, H.; Nagase, S.; Hirayama, A.; Koyama, A.; Ohya, H.; Kamada, H. In vivo temporal EPR imaging for estimating the kinetics of a nitroxide radical in the renal parenchyma and pelvis in rats. *Magn. Reson. Imaging* **2002**, *20*, 77–82. [CrossRef]

82. Hirayama, A.; Yoh, K.; Nagase, S.; Ueda, A.; Itoh, K.; Morito, N.; Hirayama, K.; Takahashi, S.; Yamamoto, M.; Koyama, A. EPR imaging of reducing activity in Nrf2 transcriptional factor-deficient mice. *Free Radic. Biol. Med.* **2003**, *34*, 1236–1242. [CrossRef]

83. Sonta, T.; Inoguchi, T.; Matsumoto, S.; Yasukawa, K.; Inuo, M.; Tsubouchi, H.; Sonoda, N.; Kobayashi, K.; Utsumi, H.; Nawata, H. In vivo imaging of oxidative stress in the kidney of diabetic mice and its normalization by angiotensin II type 1 receptor blocker. *Biochem. Biophys. Res. Commun.* **2005**, *330*, 415–422. [CrossRef] [PubMed]

84. Chen, Z.; Reyes, L.A.; Johnson, D.H.; Velayutham, M.; Yang, C.; Samouilov, A.; Zweier, J.L. Fast gated EPR imaging of the beating heart: Spatiotemporally resolved 3D imaging of free-radical distribution during the cardiac cycle. *Magn. Reson. Med.* **2013**, *69*, 594–601. [CrossRef] [PubMed]

85. Johnson, D.H.; Ahmad, R.; Liu, Y.; Chen, Z.; Samouilov, A.; Zweier, J.L. Uniform spinning sampling gradient electron paramagnetic resonance imaging. *Magn. Reson. Med.* **2014**, *71*, 893–900. [CrossRef] [PubMed]

86. Caia, G.L.; Efimova, O.V.; Velayutham, M.; El-Mahdy, M.A.; Abdelghany, T.M.; Kesselring, E.; Petryakov, S.; Sun, Z.; Samouilov, A.; Zweier, J.L. Organ specific mapping of in vivo redox state in control and cigarette smoke-exposed mice using EPR/NMR co-imaging. *J. Magn. Reson.* **2012**, *216*, 21–27. [CrossRef] [PubMed]

87. Ueda, Y.; Yokoyama, H.; Ohya-Nishiguchi, H.; Kamada, H. ESR spectroscopy for analysis of hippocampal elimination of a nitroxide radical during kainic acid-induced seizure in rats. *Magn. Reson. Med.* **1998**, *40*, 491–493. [CrossRef]

88. Miura, Y.; Anzai, K.; Takahashi, S.; Ozawa, T. A novel lipophilic spin probe for the measurement of radiation damage in mouse brain using in vivo electron spin resonance (ESR). *FEBS Lett.* **1997**, *419*, 99–102. [CrossRef]

89. Utsumi, H.; Sano, H.; Naruse, M.; Matsumoto, K.; Ichikawa, K.; Oi, T. Nitroxyl probes for brain research and their application to brain imaging. *Methods Enzymol.* **2002**, *352*, 494–506.

90. Kinoshita, Y.; Yamada, K.; Yamasaki, T.; Mito, F.; Yamato, M.; Kosem, N.; Deguchi, H.; Shirahama, C.; Ito, Y.; Kitagawa, K.; et al. In vivo evaluation of novel nitroxyl radicals with reduction stability. *Free Radic. Biol. Med.* **2010**, *49*, 1703–1709. [CrossRef]

91. Sano, H.; Naruse, M.; Matsumoto, K.; Oi, T.; Utsumi, H. A new nitroxyl-probe with high retention in the brain and its application for brain imaging. *Free Radic. Biol. Med.* **2000**, *28*, 959–969. [CrossRef]

92. Anzai, K.; Saito, K.; Takeshita, K.; Takahashi, S.; Miyazaki, H.; Shoji, H.; Lee, M.C.; Masumizu, T.; Ozawa, T. Assessment of ESR-CT imaging by comparison with autoradiography for the distribution of a blood-brain-barrier permeable spin probe, MC-PROXYL, to rodent brain. *Magn. Reson. Imaging* **2003**, *21*, 765–772. [CrossRef]

93. Diehl, K.H.; Hull, R.; Morton, D.; Pfister, R.; Rabemampianina, Y.; Smith, D.; Vidal, J.M.; van de Vorstenbosch, C. European Federation of Pharmaceutical Industries Association and European Centre for the Validation of Alternative Methods A good practice guide to the administration of substances and removal of blood, including routes and volumes. *J. Appl. Toxicol. JAT* **2001**, *21*, 15–23. [CrossRef] [PubMed]

94. Yokoyama, H.; Itoh, O.; Aoyama, M.; Obara, H.; Ohya, H.; Kamada, H. In vivo temporal EPR imaging of the brain of rats by using two types of blood-brain barrier-permeable nitroxide radicals. *Magn. Reson. Imaging* **2002**, *20*, 277–284. [CrossRef]

95. Yokoyama, H.; Ishida, S.-I.; Ogata, T. In vivo temporal EPR study using a region-selected intensity determination method to estimate cerebral reducing ability in rats treated with olanzapine. *Magn. Reson. Imaging* **2010**, *28*, 898–902. [CrossRef] [PubMed]

96. Emoto, M.C.; Sato-Akaba, H.; Hirata, H.; Fujii, H.G. Dynamic changes in the distribution and time course of blood–brain barrier-permeative nitroxides in the mouse head with EPR imaging: Visualization of blood flow in a mouse model of ischemia. *Free Radic. Biol. Med.* **2014**, *74*, 222–228. [CrossRef] [PubMed]

97. Emoto, M.C.; Yamato, M.; Sato-Akaba, H.; Yamada, K.; Matsuoka, Y.; Fujii, H.G. Brain imaging in methamphetamine-treated mice using a nitroxide contrast agent for EPR imaging of the redox status and a gadolinium contrast agent for MRI observation of blood-brain barrier function. *Free Radic. Res.* **2015**, *49*, 1038–1047. [CrossRef] [PubMed]

98. Matsumura, A.; Emoto, M.C.; Suzuki, S.; Iwahara, N.; Hisahara, S.; Kawamata, J.; Suzuki, H.; Yamauchi, A.; Sato-Akaba, H.; Fujii, H.G.; et al. Evaluation of oxidative stress in the brain of a transgenic mouse model of Alzheimer disease by in vivo electron paramagnetic resonance imaging. *Free Radic. Biol. Med.* **2015**, *85*, 165–173. [CrossRef]

99. Fang, D.; Zhang, Z.; Li, H.; Yu, Q.; Douglas, J.T.; Bratasz, A.; Kuppusamy, P.; Yan, S.S. Increased electron paramagnetic resonance signal correlates with mitochondrial dysfunction and oxidative stress in an Alzheimer's disease mouse brain. *J. Alzheimers Dis.* **2016**, *51*, 571–580. [CrossRef]

100. Emoto, M.C.; Matsuoka, Y.; Yamada, K.-I.; Sato-Akaba, H.; Fujii, H.G. Non-invasive imaging of the levels and effects of glutathione on the redox status of mouse brain using electron paramagnetic resonance imaging. *Biochem. Biophys. Res. Commun.* **2017**, *485*, 802–806. [CrossRef]

101. Emoto, M.C.; Sato-Akaba, H.; Matsuoka, Y.; Yamada, K.-I.; Fujii, H.G. Non-invasive mapping of glutathione levels in mouse brains by in vivo electron paramagnetic resonance (EPR) imaging: Applied to a kindling mouse model. *Neurosci. Lett.* **2018**, *690*, 6–10. [CrossRef]

102. Paletta, J.T.; Pink, M.; Foley, B.; Rajca, S.; Rajca, A. Synthesis and reduction kinetics of sterically shielded pyrrolidine nitroxides. *Org. Lett.* **2012**, *14*, 5322–5325. [CrossRef] [PubMed]

103. Jagtap, A.P.; Krstic, I.; Kunjir, N.C.; Hänsel, R.; Prisner, T.F.; Sigurdsson, S.T. Sterically shielded spin labels for in-cell EPR spectroscopy: Analysis of stability in reducing environment. *Free Radic. Res.* **2015**, *49*, 78–85. [CrossRef] [PubMed]

104. Emoto, M.; Mito, F.; Yamasaki, T.; Yamada, K.-I.; Sato-Akaba, H.; Hirata, H.; Fujii, H. A novel ascorbic acid-resistant nitroxide in fat emulsion is an efficient brain imaging probe for in vivo EPR imaging of mouse. *Free Radic. Res.* **2011**, *45*, 1325–1332. [CrossRef] [PubMed]

105. Emoto, M.C.; Yamada, K.-I.; Yamato, M.; Fujii, H.G. Novel ascorbic acid-resistive nitroxide in a lipid emulsion: An efficient brain imaging contrast agent for MRI of small rodents. *Neurosci. Lett.* **2013**, *546*, 11–15. [CrossRef] [PubMed]

106. Wang, X.; Emoto, M.; Miyake, Y.; Itto, K.; Xu, S.; Fujii, H.; Hirata, H.; Arimoto, H. Novel blood-brain barrier-permeable spin probe for in vivo electron paramagnetic resonance imaging. *Bioorg. Med. Chem. Lett.* **2016**, *26*, 4947–4949. [CrossRef] [PubMed]

107. Khramtsov, V.V. In vivo molecular electron paramagnetic resonance-based spectroscopy and imaging of tumor microenvironment and redox using functional paramagnetic Probes. *Antioxid. Redox Signal.* **2018**, *28*, 1365–1377. [CrossRef] [PubMed]

108. Goodwin, J.; Yachi, K.; Nagane, M.; Yasui, H.; Miyake, Y.; Inanami, O.; Bobko, A.A.; Khramtsov, V.V.; Hirata, H. In vivo tumour extracellular pH monitoring using electron paramagnetic resonance: The effect of X-ray irradiation. *NMR Biomed.* **2014**, *27*, 453–458. [CrossRef]

109. Biller, J.R.; Tseitlin, M.; Mitchell, D.G.; Yu, Z.; Buchanan, L.A.; Elajaili, H.; Rosen, G.M.; Kao, J.P.Y.; Eaton, S.S.; Eaton, G.R. Improved sensitivity for imaging spin trapped hydroxyl radical at 250 MHz. *ChemPhysChem* **2015**, *16*, 528–531. [CrossRef]

110. Tan, X.; Tao, S.; Liu, W.; Rockenbauer, A.; Villamena, F.A.; Zweier, J.L.; Song, Y.; Liu, Y. Synthesis and characterization of the perthiatriarylmethyl radical and its dendritic derivatives with high sensitivity and selectivity to superoxide radical. *Chem. Eur. J.* **2018**, *24*, 6958–6967. [CrossRef]

111. Poncelet, M.; Driesschaert, B.; Bobko, A.A.; Khramtsov, V.V. Triarylmethyl-based biradical as a superoxide probe. *Free Radic. Res.* **2018**, *52*, 373–379. [CrossRef]

112. Decroos, C.; Li, Y.; Bertho, G.; Frapart, Y.; Mansuy, D.; Boucher, J.-L. Oxidation of tris-(p-carboxyltetrathiaaryl)methyl radical EPR probes: Evidence for their oxidative decarboxylation and molecular origin of their specific ability to react with O_2^{*-}. *Chem. Commun.* **2009**, 1416–1418. [CrossRef] [PubMed]

113. Bobko, A.A.; Efimova, O.V.; Voinov, M.A.; Khramtsov, V.V. Unique oxidation of imidazolidine nitroxides by potassium ferricyanide: Strategy for designing paramagnetic probes with enhanced sensitivity to oxidative stress. *Free Radic. Res.* **2012**, *46*, 1115–1122. [CrossRef] [PubMed]

114. Glazachev, Y.I.; Grigor'ev, I.A.; Reijerse, E.J.; Khramtsov, V.V. EPR studies of 15N- and 2H-substituted pH-sensitive spin probes of imidazoline and imidazolidine types. *Appl. Magn. Reson.* **2001**, *20*, 489–505. [CrossRef]

115. Bobko, A.A.; Kirilyuk, I.A.; Gritsan, N.P.; Polovyanenko, D.N.; Grigor'ev, I.A.; Khramtsov, V.V.; Bagryanskaya, E.G. EPR and quantum chemical studies of the pH-sensitive imidazoline and imidazolidine nitroxides with bulky substituents. *Appl. Magn. Reson.* **2010**, *39*, 437–451. [CrossRef] [PubMed]